10726 *Inorg. Chem.* **2009**, *48*, 10726–10736
DOI: 10.1021/ic901615e

Inorganic Chemistry
Article

Consecutive Irreversible Single-Crystal to Single-Crystal and Reversible Single-Crystal to Glass Transformations and Associated Magnetism of the Coordination Polymer, $[Mn^{II}(rac\text{-pnH})(H_2O)Cr^{III}(CN)_6]\cdot H_2O$

Yusuke Yoshida,[†] Katsuya Inoue,*[,†] and Mohamedally Kurmoo*[,‡]

[†]*Department of Chemistry and Institute for Advanced Materials Research, Hiroshima University, Kagamiyama, Higashi-Hiroshima, 739-8526, Japan, and* [‡]*Laboratoire de Chimie de Coordination Organique, CNRS-UMR7140, Université de Strasbourg, Institut Le Bel, 4 rue Blaise Pascal, 67000 Strasbourg Cedex 01, France*

Received August 12, 2009

The achiral coordination polymer $[Mn^{II}(rac\text{-pnH})(H_2O)Cr^{III}(CN)_6]\cdot H_2O$, (*rac*-pn = racemic 1,2-diaminopropane), $\mathbf{1}\cdot 2H_2O$, has been prepared, and its crystal structures, optical and magnetic properties have been studied before and after dehydration followed by rehydration. The in situ X-ray diffraction, performed on one selected single crystal, shows an unusual irreversibility from the as-prepared $\mathbf{1}\cdot 2H_2O$ to the dehydrated $[Mn(rac\text{-pnH})Cr(CN)_6]$, **1**, and reversibility from **1** to rehydrated $[Mn(rac\text{-pnH})(H_2O)Cr(CN)_6]\cdot H_2O$ **1-HP**. Virgin $\mathbf{1}\cdot 2H_2O$ crystallizes in the monoclinic achiral $P2_1/m$ space-group having a two-dimensional (2D) square-network of Mn−Cr with bridging cyanide, and behaves as a soft ferrimagnet (T_C = 36 K). Dehydrated **1** has a three-dimensional (3D) network with an additional cyanide bridge between layers and adopts the orthorhombic achiral *Pmnb* space-group exhibiting a ferrimagnetic behavior (T_C = 70 K). Rehydrated **1-HP** (T_C = 36 K) is poorly crystallized having the same unit-cell as $\mathbf{1}\cdot 2H_2O$ and reversibly transforms to the crystalline **1** (T_C = 70 K). The dehydration is associated to a change in the coordination of the amine from one layer to its neighboring one involving a proton transfer, going from $\{Mn\text{-}NH_2CH(CH_3)CH_2N'H_3^+\cdots\cdots(H_2O)Mn'\}$ for $\mathbf{1}\cdot 2H_2O$ to $\{Mn\text{-}NC\cdots\cdots NH_3^+CH(CH_3)CH_2H_2N'-Mn'\}$ for **1**. The irreversible transformation of virgin single crystal $\mathbf{1}\cdot 2H_2O$ to single-crystal **1** is promoted by the availability of only one Mn in the vicinity of the cyanide while during the rehydration process the reversible single-crystal **1** to a glassy **1-HP** is due to the presence of two equidistant Mn atoms, which is the cause of the disorder. The change in magnetism, that is, the increase of the Curie temperature and coercive field, is associated to the structural transformation from 2D to 3D.

Introduction

The transformation between different states of matter, for example the melting of snow or white to red phosphorus, is among the most fascinating physical phenomena one can experience, and it always leave the curious ones with the question "How does it take place?".[1] Therefore unraveling the characteristics of the mechanism and the energetics involved in such transformations is a major goal.[2] The transformation sometimes gives the materials their particular characteristics and functions and consequently, their applications. Therefore, a thorough understanding of such transformation forms an important integral step in the development of new functional materials.[3] The usual first step is to elucidate the structures in the different states. As such, structural phase transitions for many solid-to-solid transformations of materials, which retain the same atomic or molecular contents in all their states, have been well studied. For example, silicon changes its structure from diamond to β-Sn to simple hexagonal to hexagonal close packed under pressure while the more complex $[NH(CH_3)_3]CdCl_3$ changes from an orthorhombic phase (*Pbnm*) to hexagonal ($P6_3/m$, $Z = 18$) at 342 K and to another hexagonal ($P6_3/m$, $Z = 6$) at 374 K.[4,5] When there are changes in the contents, for example, the loss of

*To whom correspondence should be addressed. E-mail: kxi@hiroshima-u.ac.jp (K.I.), kurmoo@chimie.u-strasbg.fr (M.K.). Phone: (+81) 82-424-7416 (K.I.), (+33) 3 6885 1356 (M.K.). Fax: (+81) 82-424-7416 (K.I.), (+33) 3 6885 1325 (M.K.).

(1) Bragg, W. L. *Christmas Lectures series "The Nature of Things"*; 1962; http://www.rigb.org/contentControl?action=displayContent&id=00000000610.

(2) (a) Stanley, H. E. *Phase transitions and critical phenomena*; Clarendon Press, OUP: Oxford, 1971. (b) *Phase transitions*; Cross, L. E., Ed.; Pergamon: New York, 1973.

(3) (a) Special issue on "Metal-Organic-Frameworks"; Long, J. R., Yaghi, O. M., Eds.; *Chem. Soc. Rev.*, **2009**, *38*(5). (b) *Special Publication Royal Society of Chemistry, Metal-Organic and Organic Molecular Magnets*; Day, P., Underhill, A. E. Eds.; **2000**, Vol. *252*. (c) Rao, C. N. R.; Cheetham, A. K.; Thirumurugan, A. *J. Phys.: Condens. Matter* **2008**, *20*, 083202. (d) Blundell, S. J.; Pratt, F. L. *J. Phys.:Condens. Matter* **2004**, *16*, R771.

(4) Madelung, O. *Semiconductors: Data handbook*, 3rd ed; Birkhäuser: Germany, 2004; p16.

(5) Chapuis, G.; Zuniga, J. *Acta Crystallogr.* **1980**, *B36*, 807.

 Published on Web 10/09/2009

solvents from a crystal, the stability of the structures can be greatly affected and in many cases, the transformation is accompanied by a loss of crystallinity.[6] Recently, this general view is being revised because of the exponential progress made in the field of metal-organic frameworks which has delivered many examples of crystals-to-crystal transformation upon desolvation.[7] The associated physical properties have also been of great interest in view of the development of functional materials that can be used as detectors. These properties can be long-range magnetic orderings, spin crossover, luminescence and dielectricity.[3] Of utmost importance, in the present energy conservation and climate control era, is the retention of fuel gases/liquids especially that of hydrogen molecules in the pores of the frameworks or the selective adsorption of unwanted or noxious gases such as CO_2 and NOX.[8] Much progress has been made so far in the synthesis and characterization of porous frameworks, and many framework materials are being tested before application can be envisaged.[9]

In the past few years, there has been an increase in the development of porous magnets, prompted by a purely academic interest and the challenge that magnetic ordering is not generally favored by magnetic exchange between distant moment carriers through space, that display reversible single-crystal to single-crystal transformation upon desolvation and resolvation.[10] This increase in activities has given rise to several magnetic compounds being sensitive to their solvent contents. For example, dehydration of the pillared layered cobalt hydroxide, $Co_5(OH)_8(chdc).4H_2O$ (chdc = 1,4-cyclohexanedicarboxylate),[11] has little effect on the magnetic properties while for the series $M^{II}_3(HCOO)_6$.solvent (M = Mn, Co, Ni, or Fe and S can be one of many solvents or gases) the Curie temperature varies depending on the solvent molecule.[12] On the other hand, the antiferromagnetic $Co_3(OH)_2(C_4O_4)_2\cdot 3H_2O$ transforms reversibly to the ferromagnetic $Co_3(OH)_2(C_4O_4)_2$, and ferrimagnetic $Ni_3(OH)_2(chdc)_2(H_2O)_4\cdot 3H_2O$ become ferromagnetic upon partial dehydration.[13,14] More exotic examples are known where the temperature of high-spin to low-spin transition is altered, or the magnetic behaviors changes from being long-range ordered to low-dimensional or the Curie temperature is controlled by the amount of water in the solid or by the solvent that is trapped in the pores.[15−18]

The family of compounds, $[M^{II}(L)(H_2O)M^{III}(CN)_6]\cdot H_2O$ where M^{II} = Mn and M^{III} = Cr or Mn and *L* is an alkyldiamineH^+, originally studied in the search for existing synergy between chirality and magnetism, has proved to be very rich in the range of crystal chemistry behaviors upon dehydration.[19−32] Reversible single-crystal to single-crystal

(6) (a) Yanai, N.; Kaneko, W.; Yoneda, K.; Ohba, M.; Kitagawa, S. *J. Am. Chem. Soc*. **2007**, *129*, 3496. (b) Maspoch, D.; Ruiz-Molina, D.; Wurst, K.; Domingo, N.; Gavallini, M.; Biscarini, F.; Tajada, J.; Rovira, C.; Veciana, J. *Nat. Mater*. **2003**, *2*, 190. (c) Sun, R.; Li, Y.-Z.; Bai, J.; Pan, Y *Cryst. Growth Des*. **2007**, *7*, 890.

(7) (a) Barbour, L. J. *Aust. J. Chem*. **2006**, *59*, 595. (b) Vittal, J. J. *Coord. Chem. Rev*. **2007**, *251*, 1781. (c) Kepert, C. J. *Chem. Commun*. **2006**, 695.

(8) (a) Dinca, M.; Long, J. R. *Angew. Chem., Int. Ed*. **2008**, *47*, 2. (b) Murray, L. J.; Dinca, M.; Long, J. R. *Chem. Soc. Rev*. **2009**, *38*, 1294. (c) Zhao, X.; Xiao, B.; Fletcher, A. J.; Thomas, K. M.; Bradshaw, D.; Rosseinsky, M. J. *Science* **2004**, *306*, 1012. (d) Chen, B.; Ockwig, N. W.; Millward, A. R.; Contreras, D. S.; Yaghi, O. M. *Angew. Chem., Int. Ed*. **2005**, *44*, 4745. (e) Li, J.-R.; Kuppler, R. J.; Zhou, H.-C. *Chem. Soc. Rev*. **2009**, *38*, 1477.

(9) (a) Batten, S. R.; Robson, R. *Angew. Chem., Int. Ed*. **1998**, *110*, 1558. (b) Yaghi, O. M. *Acc. Chem. Res*. **2005**, *38*, 176. (c) Robson, R. *J. Chem. Soc., Dalton Trans*. **2000**, 3735. (d) Kitagawa, S.; Kitaura, R.; Noro, S. *Angew. Chem., Int. Ed*. **2004**, *43*, 2334. (e) Uemura, T.; Horike, S.; Kitagawa, S. *Chem. Asian. J*. **2006**, *1*, 36. (f) Kitagawa, S.; Uemura, K. *Chem. Soc. Rev*. **2005**, *34*, 109. (g) Bradshaw, D.; Claridge, J. B.; Cussen, E. J.; Prior, T. J.; Rosseinsky, M. J. *Acc. Chem. Res*. **2005**, *38*, 273. (h) Wang, Z.; Zhang, Y.; Kurmoo, M.; Liu, T.; Vilminot, S.; Zhao, B.; Gao, S. *Aust. J. Chem*. **2006**, *59*, 617.

(10) Kurmoo, M. *Chem. Soc. Rev*. **2009**, *38*, 1353.

(11) Kumagai, H.; Kepert, C. J.; Kurmoo, M. *Inorg. Chem*. **2002**, *41*, 3410.

(12) (a) Wang, Z.-M.; Zhang, B.; Fujiwara, H.; Kobayashi, H.; Kurmoo, M. *Chem. Commun*. **2004**, 416. (b) Wang, Z.-M.; Zhang, B.; Kurmoo, M.; Green, M. A.; Fujiwara, H.; Otsuka, T.; Kobayashi, H. *Inorg. Chem*. **2005**, *44*, 1230. (c) Wang, Z.-M.; Zhang, Y.; Liu, T.; Kurmoo, M.; Gao, S. *Adv. Funct. Mater*. **2007**, *17*, 1523. (d) Wang, Z.-M.; Zhang, B.; Zhang, Y.; Kurmoo, M.; Liu, T.; Gao, S.; Kobayashi, H. *Polyhedron* **2007**, *26*, 2207. (e) Zhang, B.; Wang, Z.-M.; Kurmoo, M.; Gao, S.; Inoue, K.; Kobayashi, H. *Adv. Funct. Mater*. **2007**, *17*, 577. (f) Stride, J. A.; Kurmoo, M.; Wang, Z.-M. *Physica B: Condensed Matter* **2006**, *385*−*386*, 465. (g) Wang, Z.-M.; Zhang, Y.; Liu, T; Kurmoo, M.; Gao, S. H. *Adv. Funct. Mater*. **2007**, *17*, 1523.

(13) Kurmoo, M.; Kumagai, H.; Chapman, K. W.; Kepert, C. J. *Chem. Commun*. **2005**, 3012. (b) Gutcshke, S. O. H.; Molinier, M.; Powell, A. K.; Wood, P. T. *Angew. Chem., Int. Ed. Engl*. **1997**, *36*, 991.

(14) Kurmoo, M.; Kumagai, H.; Akita-Tanaka, M.; Inoue, K.; Takagi, S. *Inorg. Chem*. **2006**, *45*, 1627.

(15) Halder, G. J.; Kepert, C. J.; Moubaraki, B.; Murray, K. S.; Cashion, J. D. *Science* **2002**, *298*, 1762. (b) Galet, A.; Muñoz, M. C.; Real, J. A. *Chem. Commun*. **2006**, 4321. (c) Niel, V.; Thompson, A. L.; Munoz, M. C.; Galet, A.; Goeta, A. E.; Real, J. A. *Angew. Chem., Int. Ed*. **2003**, *42*, 3759. (d) Duriska, M. B.; Neville, S. M.; Moubaraki, B.; Cashion, J. D.; Halder, G. J.; Chapman, K. W.; Balde, C.; Létard, J.-F.; Murray, K. S.; Kepert, C. J.; Batten, S. R. *Angew. Chem., Int. Ed*. **2009**, *48*, 2428. (e) Coppens, P. *Angew. Chem., Int. Ed*. **2009**, *48*, 4280.

(16) (a) Ohkoshi, S.; Arai, K.; Sato, Y.; Hashimoto, K. *Nat. Mat*. **2004**, *3*, 857. (b) Ohkoshi, S.; Tsunobuchi, Y.; Takahashi, H.; Hozumi, T.; Shiro, M.; Hashimoto, K. *J. Am. Chem. Soc*. **2007**, *129*, 3084.

(17) (a) Nihei, M.; Han, L.; Oshio, H. *J. Am. Chem. Soc*. **2007**, *129*, 5312. (b) Zeng, M.-H.; Feng, Z.-L.; Zhang, W.-X.; Chen, Z.-M. *Dalton Trans*. **2006**, 5294. (c) Liu, Y.-H.; Tsai, H.-L.; Lu, Y.-L.; Wen, Y.-S.; Wang, J.-C.; Lu, K.-L. *Inorg. Chem*. **2001**, *40*, 6426. (d) Cheng, X.-N.; Zhang, W.-X.; Lin, Y.-Y.; Zheng, Y.-Z.; Chen, X.-M. *Adv. Mater*. **2007**, *19*, 1494. (e) Cheng, X.-N.; Zhang, W.-X.; Lin, Y.-Y.; Zheng, Y.-Z.; Chen, X.-M. *Adv. Mater*. **2007**, *19*, 1494. (f) Zhang, X.-M.; Hao, Z.-M.; Zhang, W.-X.; Chen, X.-M. *Angew. Chem., Int. Ed*. **2007**, *119*, 3526. (g) Li, Z.-G.; Wang, G.-H.; Jia, H.-Q.; Hu, N.-H.; Xu, J.-W. *CrystEngComm* **2008**, *10*, 173. (h) Zeng, M.-H.; Feng, X.-L.; Zhang, W.-X.; Chen, X.-M. *Dalton Trans*. **2006**, 5294. (i) Xiang, S.; Wu, X.; Zhang, J.; Fu, R.; Hu, S.; Zhang, X. *J. Am. Chem. Soc*. **2005**, *127*, 16352.

(18) Murrie, M.; Teat, S. J.; Stœckli-Evans, H.; Güdel, H. U. *Angew. Chem., Int. Ed*. **2003**, *42*, 4653.

(19) Imai, H.; Inoue, K.; Kikuchi, K.; Yoshida, Y.; Ito, M.; Sunahara, T.; Onaka, S. *Angew. Chem., Int. Ed*. **2004**, *43*, 5618.

(20) (a) Akita-Tanaka, M.; Kumagai, H.; Markosyan, A.; Inoue, K. *Bull. Chem. Soc. Jpn*. **2007**, *80*, 204. (b) Numata, Y.; Inoue, K.; Baranov, N.; Kurmoo, M.; Kikuchi, K. *J. Am. Chem. Soc*. **2007**, *129*, 9902. (c) Munguet, M.; Luneau, D.; Lhotel, E.; Villar, V.; Paulsen, C.; Amabilino, D. B.; Veciana, J. *Angew. Chem., Int. Ed*. **2002**, *41*, 586. (d) Kumagai, H.; Inoue, K. *Angew. Chem., Int. Ed*. **1999**, *38*, 1601.

(21) (a) Milon, J.; Daniel, M.-C.; Kaiba, A.; Guionneau, P.; Brandès, S.; Sutter, J.-P. *J. Am. Chem. Soc*. **2007**, *129*, 13872. (b) Higashikawa, H.; Okuda, K.; Kishine, J.; Masuhara, N.; Inoue, K. *Chem. Lett*. **2007**, *36*, 1022. (d) Coronado, E.; Gómez-García, C. J.; Nuez, A.; Romeo, F. M.; Rusanov, E.; Stoeckli-Evans, H. *Inorg. Chem*. **2002**, *41*, 4615. (e) Inoue, K.; Imai, H.; Ghalsasi, P. S.; Kikuchi, K.; Ohba, M.; Okawa, H.; Yakhmi, J. V. *Angew. Chem., Int. Ed*. **2001**, *40*, 4242.

(22) (a) Coronado, E.; Galán-Mascarós, J. R.; Gómez-García, C. J.; Mursia-Martínez, A. *Chem.—Eur. J*. **2006**, *12*, 3484. (b) Zeng, M.-H.; Wang, B.; Wang, X.-Y.; Zhang, W.-X.; Chen, X.-M.; Gao, S. *Inorg. Chem*. **2006**, *45*, 7069.

(23) Rikken, G. L. J. A.; Raupach, E. *Nature*. **1997**, *390*, 493.

(24) (a) Blokhin, I. V.; Markosyan, A. S.; Morgunov, R. B.; Inoue, K.; Tanimoto, Y.; Yoshida, Y. *Phys. Solid State* **2005**, *47*, 2106. (b) Hoshikawa, A.; Kamiyama, T.; Purwanto, A.; Ohishi, K.; Higemoto, W.; Ishigaki, T.; Imai, H.; Inoue, K. *J. Phys. Soc. Jpn*. **2004**, *73*, 2597. (c) Ohishi, K.; Higemoto, W.; Koda, A.; Saha, S. R.; Kadono, R.; Inoue, K.; Imai, H.; Higasikawa, H. *J. Phys. Soc. Jpn*. **2006**, *75*, 063705.

(25) Inoue, K.; Kikuchi, K.; Ohba, M.; Okawa, H. *Angew. Chem., Int. Ed*. **2003**, *42*, 4810.

(26) Kishine, J.; Inoue, K.; Yoshida, Y. *Prog. Theor. Phys. Suppl*. **2005**, 82.

(27) (a) Yoshida, Y.; Inoue, K.; Kurmoo, M. *Chem. Lett*. **2008**, *37*, 504. (b) Yoshida, Y.; Inoue, K.; Kurmoo, M. *Inorg. Chem*. **2009**, *48*, 267.

(28) Yoshida, Y.; Inoue, K.; Kurmoo, M. *Chem. Lett*. **2008**, *37*, 586.

(29) Kaneko, W.; Ohba, M.; Kitagawa, S. *J. Am. Chem. Soc*. **2007**, *129*, 248.

(30) Kaneko, W.; Ohba, M.; Kitagawa, S. *J. Am. Chem. Soc*. **2007**, *129*, 13706.

(31) Mito, M.; Iriguchi, K.; Deguchi, H.; Kishine, J.; Kikuchi, K.; Ohsumi, H.; Yoshida, Y.; Inoue, K. *Phys. Rev. B* **2009**, *79*, 012406.

(32) Yoshida, Y. PhD Thesis, Hiroshima University, Japan, **2008**.

as well as single-crystal to glass behaviors have been encountered.[27−30] On one hand the chiral [Mn(*R*-pnH)(H_2O)Cr($CN)_6$]·H_2O (**2R**·$2H_2O$) remains crystalline in all its forms and displays complete structural reversibility.[32] On the other hand for the achiral [Mn(enH)(H_2O)Cr($CN)_6$]·H_2O (**3**·$2H_2O$), the virgin crystal becomes glassy upon dehydration and recovers its crystallinity partially when rehydrated.[27] [Mn(*rac*-pnH)(H_2O)Cr($CN)_6$]·H_2O displays a different behavior to the two cases above. For every system, the Curie temperature is nearly doubled upon dehydration and reverses upon rehydration. Here, we present an extended account of the in situ studies of the crystal chemistry of [Mn(*rac*-pnH)(H_2O)Cr($CN)_6$]·H_2O and its associated thermal, optical and magnetic properties in all its forms.[28] In addition we propose a mechanism to understand the reversible and irreversible processes.

Experimental Section

Synthesis of *rac*-pn·2HCl. Seven milliliters (6.12 g, 82.6 mmol) of *rac*-1,2-diaminopropane (d = 0.87 g/mL) was added to 13.6 mL (16.5 g, 167 mmol) of 37% HCl (d = 1.19 g/mL). The mixture was evaporated to yield a white powder. It was then dissolved in a minimum amount of hot water. The concentrated hot solution was cooled to room temperature and then added to EtOH while stirring until no precipitation occurs. The precipitate was filtered and washed with EtOH and ether. Yield 7.55 g, 62%.[32]

Synthesis of [Mn(*rac*-pnH)(H_2O)][Cr($CN)_6$]·H_2O (1·$2H_2O$). This coordination polymer was prepared according to the reported procedures.[28,32] Anal. Calcd (%) for 1·$2H_2O$, $C_9H_{15}CrMnN_8O_2$: C, 28.89; H, 4.04; N, 29.94. Found (%): C, 28.84; H, 4.37; N, 29.97.

Elemental Analyses. Elemental analyses for C, H, and N were performed on a Perkin-Elmer 2400II at the Natural Science Center for Basic Research and Development (N-BARD), Hiroshima University.

Infrared Spectroscopy. Infrared spectra were recorded by transmission through KBr disks containing about 0.5% of the compounds using a HORIBA FT-IR spectrometer FT-720. For **1** powdered KBr containing the virgin sample was placed under vacuum at 383 K for 2 h, and then pressed into disk. For hydrated **1-HP**, the virgin sample was heated to 365 K at a rate of 1 K/min, exposed to air overnight, then mixed with KBr and pressed into disk. For dehydrated **1** (from **1-HP**), powdered KBr containing **1-HP** was dehydrated at 383 K for 2 h.

Magnetic Measurements. Magnetic measurements were carried out by use of a Quantum Design MPMS-5S SQUID magnetometer. Diamagnetic corrections, −1.891, −1.631, −1.891, and -1.631×10^{-4} cm^3 mol^{-1} for 1·$2H_2O$, dehydrated **1**, hydrated **1-HP**, and dehydrated **1** (from **1-HP**) respectively, were estimated using Pascal constants,[33] and background correction by using the experimental measured data of an empty gelatin capsule.

Magnetic properties of polycrystalline samples for 1·$2H_2O$ were collected in part by in situ measurements. The sample of 1·$2H_2O$ was transformed in situ to **1** by heating it from 310 to 360 K at a warming rate of 0.5 K/min under a flow of helium, and then it was rehydrated ex-situ to **1-HP** by exposure to air for 1 month. **1-HP** was dehydrated by heating from 310 to 360 K at a warming rate of 0.5 K/min under a flow of helium in the SQUID magnetometer. The completion of the transformation in each case was verified by locating the critical temperature of the magnetic transition.

Zero-field-cooled (ZFC) and field-cooled (FC) magnetization measurements were performed in an applied field of 5 Oe and magnetic susceptibilities were obtained on cooling in an applied field of about 100 Oe for all phases. The field was calibrated with a Pd standard for each set of measurements. For the sample of dehydrated **1**, the magnetic susceptibility was collected on cooling from 360 to 2 K. For the other phases, magnetic susceptibilities were collected on cooling from 300 to 2 K. Isothermal magnetization at 2 K was measured for each phase from −50 to 50 kOe. The crystals were tightly pressed in the gelatin capsule to prevent motion of the crystals in an applied magnetic field. Measurements were made on different batches under different conditions to examine the reproducibility.

Thermogravimetric and Differential Thermal Analyses. Thermogravimetric and differential thermal analyses were performed on several powdered samples of 1·$2H_2O$ using a Rigaku Instrument TG8120 operating under dry nitrogen. Complete reproducibility was encountered for all samples. The representative results reported here were obtained on a sample of 9.799 mg. For the first run, the sample was first heated from 290 to 370 K at a rate of 1 K/min, followed by cooling to 290 K at a rate of 10 K/min. After cooling the sample, it was exposed to air overnight. Recycling was examined by heating at the same rate to 370, 360, 360 K, and 360 for the second, third, fourth, and fifth run, respectively. Further measurements were performed to higher temperatures by use of a Perkin-Elmer Pyris 6 TGA operating under dry nitrogen at a heating rate of 5 °C per minute on another sample of 1·$2H_2O$ of 15.497 mg.

Differential Scanning Calorimetry. Calorimetric experiments were performed on 21.844 mg of powdered 1·$2H_2O$ using a Rigaku Instrument DSC8230 operating under nitrogen atmosphere while heating in the temperature range 300−390 K. The sample was tightly packed in an aluminum pan with a lid.

Powder X-ray Diffraction. The powder X-ray diffraction (XRD) patterns were measured on a Rigaku Rint 2000 system using Cu Kα radiation and employing a scan rate of 4.0°/minute and step of 0.02°. 1·$2H_2O$ was transformed to **1** by dehydration in a heated desiccator at 363 K under nitrogen for 10 min, and then rehydrated to **1-HP** by exposing to air for 30 min, and finally this hydrated phase was placed in a heated desiccator kept at 363 K for 10 min under nitrogen to transform into **1** again. The simulated XRD patterns were calculated from the single crystal XRD data using RIETAN-2000.[34]

Single Crystal XRD. Following the determinations of the structures of the different forms on several crystals, we decided to adopt a protocol to perform all the experiments on one single crystal especially to verify the reproducibility. All the reported measurements were therefore performed in situ on one selected single-crystal at a fixed temperature of 298 K. The sample was transformed from virgin 1·$2H_2O$ to dehydrated **1**, rehydrated **1-HP**, and dehydrated **1** (second), rehydrated **1-HP** (second) sequentially. The single crystal was glued on top of a glass fiber using Araldite, and the diffraction data were collected using a Bruker SMART-APEX diffractometer equipped with a CCD area detector and graphite-monochromated Mo Kα radiation, λ = 0.71073 Å, ω-scan mode (0.3° steps). Semiempirical absorption corrections on Laue equivalents were applied. The structures were solved by direct methods and refined by full-matrix least-squares against F^2 of all data using SHELX-97. Hydrogen atoms were included in calculated positions only for C(7) atom in virgin 1·$2H_2O$ but not for the other atoms because of the presence of static disorder. The positions of the hydrogen atoms on the water oxygen atoms were located from the different Fourier map unless the refinement is unstable. All the atoms were refined anisotropically except for hydrogen atoms.

Results and Discussion

Thermogravimetric Analyses and Differential Scanning Calorimetry. The thermogravimetric measurements of

(33) *Theory of Molecular Paramagnetism*; Mulay, L. N., Boudreaux, E., Eds.; Wiley: New York, 1976.

(34) Izumi, F.; Ikeda, T. *Mater. Sci. Forum* **2000**, *321−324*, 198.

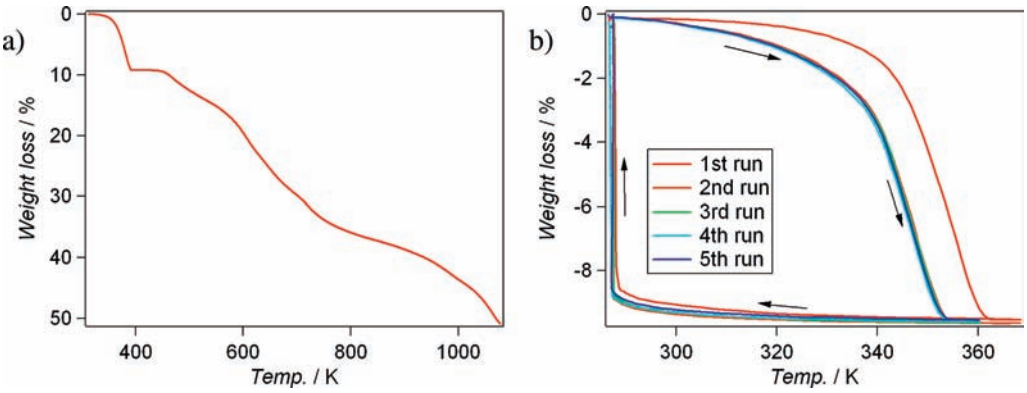

Figure 1. Thermogravimetric traces for high (a) and low (b) temperature regions for $1 \cdot 2H_2O$.

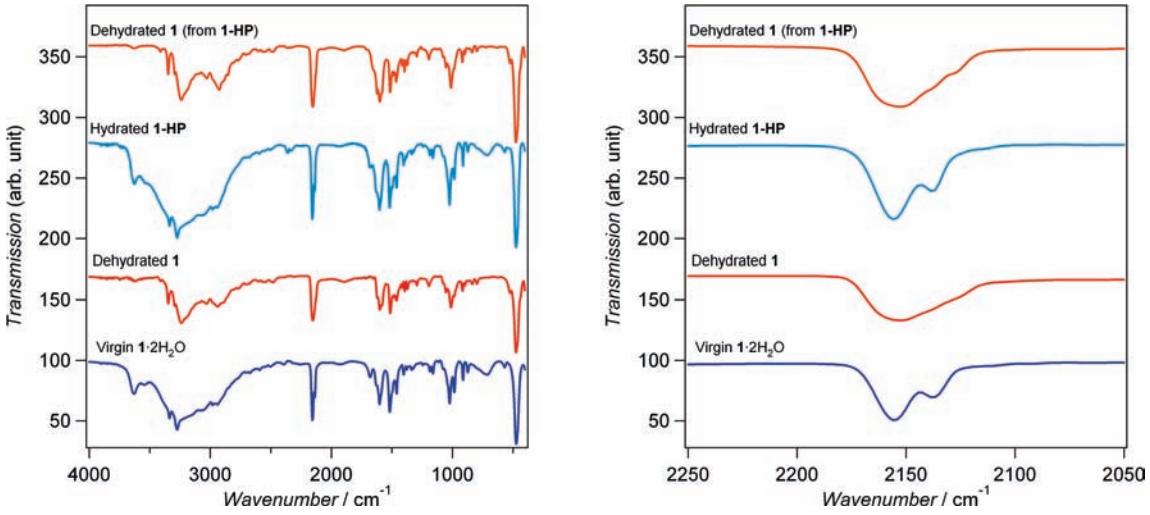

Figure 2. Infrared transmission spectra for virgin $1 \cdot 2H_2O$, dehydrated **1**, hydrated **1-HP**, and dehydrated **1** (from **1-HP**).

samples consisting of powdered crystals of $1 \cdot 2H_2O$ up to 1100 K under a nitrogen atmosphere showed a first weight loss starting at 350 K to a stable state up to 450 K where they decompose (Figure 1). There is an additional gradual weight loss from 450 K to a metastable compound at 800 K which corresponds to a mass of $MnCr(CN)_5$ and is followed by further continuous weight loss to 1100 K. For the low temperature region of the TG measurements the observed percentage weight loss (9.6%) in the first cycle is in good agreement with the departure of two water molecules per formula unit (9.63%). On lowering the temperature of the samples having been heated only to 370 K under nitrogen the weight gain is minimal. Interestingly, upon exposure of the samples to air (humidity ca. 50%) at ambient temperature for about 7 h, they reabsorb two water molecules per formula unit and recover their initial weights, which we label as **1** to hydrated **1-HP**. However, subsequent cycles were different to the first but were reproducible. This reproducibility was confirmed by repeating the cycle 4 times. The difference between the second run (and subsequent ones) to the first is that the sample loses the water molecules at a lower temperature of 340 K compared to 350 K. These results indicate that the water content in the rehydrated sample is the same as the virgin one, but the re-entrant water molecules have a reduced binding energy. The DSC curve showed a large endothermic peak starting at 360 K with a small peak around 370 K indicating the possible existence of a separate structural phase transition (Supporting Information, Figure S1). Temperature relaxation effects due to the sampling method causes a shift of the dehydration process to a higher temperature as the powdered sample was sealed in an aluminum pan with a lid.

The thermal behavior of $1 \cdot 2H_2O$ is quite different to that of $[Mn(enH)(H_2O)Cr(CN)_6] \cdot H_2O$. In the present case we find the rehydration is complete, that is, the gain in mass upon rehydration is the same as that loss for every cycle. For $[Mn(enH)(H_2O)Cr(CN)_6] \cdot H_2O$ the gain in mass is lowered and the shape of the curve changes with the number of cycle, which may be associated with fatigue.[27]

Infrared Spectroscopy. Infrared spectra of $1 \cdot 2H_2O$, dehydrated **1**, rehydrated **1-HP**, and dehydrated **1** (from **1-HP**) are shown in Figure 2. In the spectra, bands associated to H_2O, pn, and cyanide can be identified (Supporting Information, Table S1). The OH and NH stretching modes are observed above 3000 cm^{-1}. The C≡N stretching modes are observed in the range 2200−2100 cm^{-1}. The presence of two such peaks in $1 \cdot 2H_2O$ and **1-HP** may be due to bridging and terminal cyanide groups. Meanwhile only one broad peak can be seen in the spectra for dehydrated **1**. It might be an overlap of bands from four crystallographically independent

Scheme 1. Protocol Adopted for in-situ X-ray Single Crystal Structure Determinations [a]

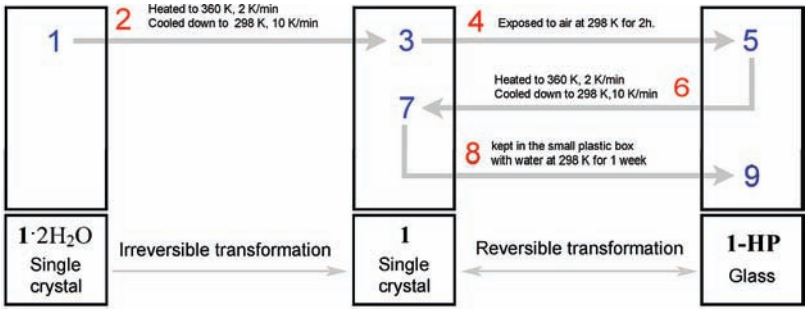

[a] Numbers in blue represent the structures (ordered for **1**, **3**, and **7** but glassy for **5** and **9**) and those in red represent the steps taken for the transformations between different states.

cyanide groups. The bending modes of H_2O and amine group of pn are seen at 1680 and 1600−1580 cm^{-1}, respectively. The bending mode of C−H, stretching mode of C−N, and bending mode of N−H are seen in the range 1520−1400, 1200−980, 920−790 cm^{-1}, respectively. The M−O and M−N bond stretch modes appear below 530 cm^{-1}. The peaks at 3631(m), 3543(vw), and 1680(w) cm^{-1} disappear after dehydration and reappear after hydration, which is consistent with their assignments to the H_2O molecule. We note that there are sharpening and shifting of some C−H and N−H bands in the spectra of dehydrated phases (**1**) compared to hydrated phase (**1**·$2H_2O$ and **1-HP**), which may be related to the presence of hydrogen bonds.

Crystal Structure. To verify the reproducibility of the changes observed in the results of TG measurements and those of structure determinations performed on several single crystals, we performed an in situ experiment using only one single-crystal for all the XRD intensity data collections and X-ray analyses of all the phases (virgin **1**·$2H_2O$, dehydrated **1**, hydrated **1-HP**, dehydrated **1**, and hydrated **1-HP**) sequentially by adopting the protocol in Scheme 1.

When the crystal of **1**·$2H_2O$ was slowly dehydrated by heating to 360 K in a flow of nitrogen, the diffraction pattern changes (see Supporting Information, movie 1). From the intensity data collected at 298 K following dehydration the crystal structure of the dehydrated phase (**1**) was successfully determined. After the data collection of the dehydrated phase, the crystal was exposed to air and the changes in the diffraction pattern were monitored for 2 h (see Supporting Information, movie 2). Unit cell parameters obtained from the observed Bragg spots for **1-HP** are almost the same as those of the virgin crystal, but the spots were too broad to realize a full and accurate crystal structure. Most surprisingly, when the rehydrated crystal was heated to 360 K, the dehydrated crystal structure was restored (see Supporting Information, movie 3). Subsequently, the crystal was kept in a small plastic box containing water at 298 K for 1 week, but the results were the same as the previous rehydrated crystal (**1-HP**). The quality of the spots was again too diffuse to permit the determination of the crystal structure. As can be seen in Scheme 1, the crystal was transformed from one state to the other repeatedly. We have listed the structure determinations by numbers in blue color and the transformation processes from one state to the other in red. The transformations have been recorded in in situ movies except for the last rehydration. We describe below the details of the structures of virgin (**1**·$2H_2O$) and dehydrated phase (**1**) and discuss the changes at the different stage.

Crystal Structure of Virgin 1·2H$_2$O. X-ray structural analysis of the diffraction data on a single crystal of **1**·$2H_2O$ suggests a $P\,2_1/m$ space-group. The key feature of the structure is the presence of two-dimensional (2D) corrugated layers parallel to the *ab*-plane and stacked along the *c*-axis (Figure 3, Table 1). The repeating unit within the anionic 2D layer consists of a bimetallic square motif of Mn(1), Cr(1), Mn(1′), and Cr(1′) ions connected by equatorial cyanide groups of the $[Cr(CN)_6]^{3-}$ ion. This is a common structural motif for this series of compounds, as exemplified by **2S**·$2H_2O$,[25] but the structures differ in space-groups and in the way the sheets are stacked which depends evidently on the nature (size, shape, stereochemistry, and chirality) of the organic ligands. The space-group for **2S**·$2H_2O$ which contains only *S*-pn is $P\,2_12_12_1$, and it is changed to $P2_1/m$ by use of a racemic mixture of pn which introduces a mirror plane on Mn atom as well as an inversion center on Cr atom. In the crystal structure of **2S**·$2H_2O$ the 2D sheets are stacked as [ABAB], where alternate layers are generated by the 2_1 symmetry along the *c*-axis. In contrast, for **1**·$2H_2O$ the 2D sheets are stacked in an eclipsed fashion [AAAA], which consequently, halved the *c*-axis found in **2S**·$2H_2O$ and changed the β angle from 90° (orthorhombic) in **2S**·$2H_2O$ to 110° (monoclinic) in **1**·$2H_2O$.

Selected bond lengths and angles are given in Table 2 and Supporting Information, Table S2. Mn ion exhibits octahedral geometry comprising nitrogen atoms from four bridging cyanide (N(1), N(2), N(1′), and N(2′)) of $[Cr(CN)_6]^{3-}$ in the equatorial positions, one nitrogen atom (N(6)) from pnH and oxygen atom (O(1)) of water molecules. The Mn(1)−N(6) distance, 2.307(4) Å, is longer than the other Mn−N distances (2.212(2)−2.225(2) Å), describing slightly distorted octahedral geometry with one elongated bond. The Cr is also distorted from a perfect octahedron with Cr−C distances in the range 2.059(3)−2.075(3) Å and C−Cr−C angles in the range 88.13(11)−91.87(11)°.

Within the 2D sheet the average separation between the Mn and Cr atoms through CN bridges is 5.3729(11) Å for **1**·$2H_2O$ which is slightly longer than that for **2S**·$2H_2O$ (5.3356(19) Å). The shortest intersheet metal−metal separation for **1**·$2H_2O$ is observed between the Mn and Cr atoms (7.5376(11) Å), while the shortest intersheet

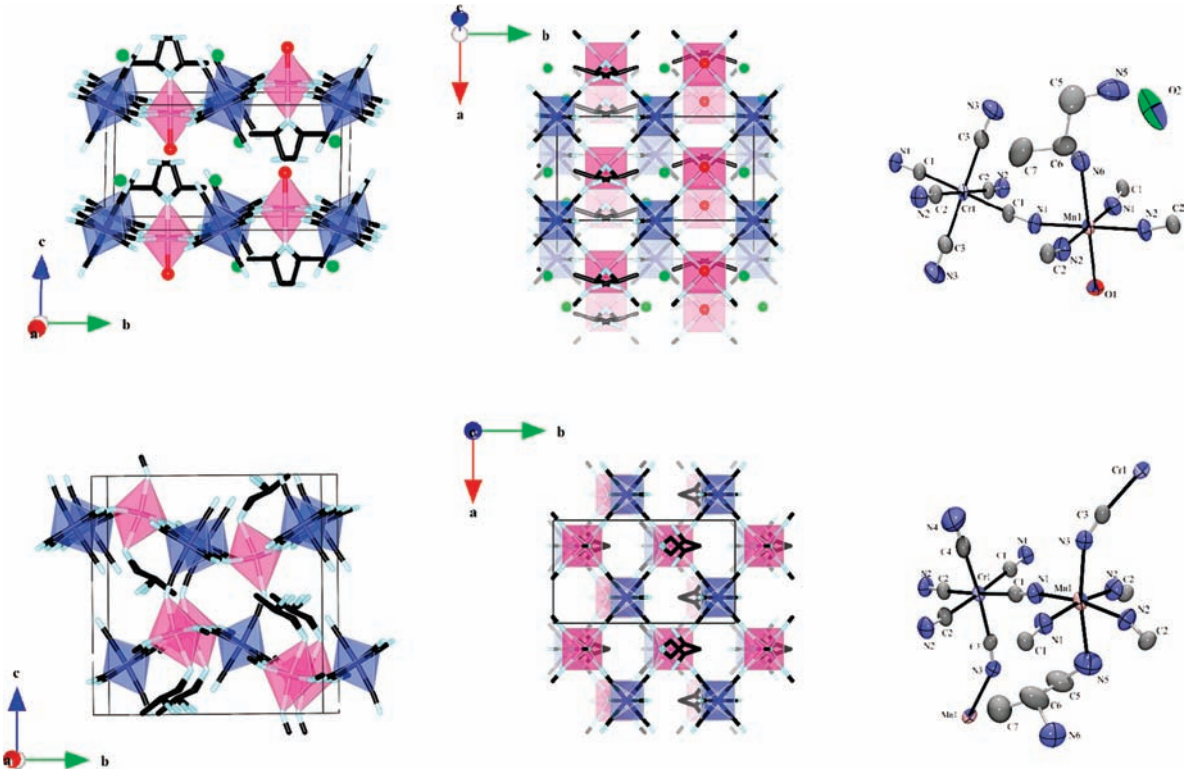

Figure 3. Projection of the crystal structures viewed along the *a*-axis (left), *c**-axis (middle), and ORTEP drawing for **1**·2H_2O (top) and **1** (bottom). The green and red balls represent the oxygen atoms of the non-coordinated and the coordinated water molecules, respectively.

Table 1. Crystallographic Data for Virgin **1**·2H_2O, Dehydrated **1**, Hydrated **1-HP**, Dehydrated **1**, and Hydrated **1-HP**

	1·2H_2O (**1**)[a]	**1**[b] (**3**)[a]	**1-HP**[c] (**5**)[a]	**1**[d] (**7**)[a]	**1-HP**[e] (**9**)[a]
formula	C9H15CrMnN8O2	C9H11CrMnN8	C9H15CrMnN8O2	C9H11CrMnN8	C9H15CrMnN8O2
fw	374.23	338.20	374.23	338.20	374.23
T, K	298	298	298	298	298
atmosphere	air	nitrogen	air	nitrogen	air
crystal system	monoclinic	orthorhombic	monoclinic	orthorhombic	monoclinic
space-group	$P2_1/m$	*Pmnb*[g]		*Pmnb*[g]	
a, Å	7.6945(14)	7.730(4)	7.631(5)	7.7245(12)	7.696(4)
b, Å	14.543(3)	13.627(7)	14.430(9)	13.609(2)	14.556(8)
c, Å	7.9749(14)	14.064(7)	7.925(5)	14.061(2)	7.996(4)
β	110.918(3)	90	110.958(11)	90	110.941(9)
V, Å^3	833.6(3)	1481.4(14)	815.0(9)	1478.1(4)	836.6(8)
Z	2	4		4	
D_C, g/cm^3	1.491	1.516		1.520	
μ (Mo Kα), mm^{-1}	1.424	1.584		1.588	
crystal size, mm^3	0.5 × 0.2 × 0.05	0.5 × 0.2 × 0.05	0.5 × 0.2 × 0.05	0.5 × 0.2 × 0.05	0.5 × 0.2 × 0.05
T_{min} and T_{max}	0.7364, 1.0000	0.7775, 1.0000		0.7891, 1.0000	
θ_{min} and θ_{max}, deg	2.734, 27.66	2.896, 24.14		2.994, 25.18	
total no. of reflections	4042	4755		6945	
no. of unique reflections (R_{int})	1916	1764		1792	
no. of observed [$I \geq 2\sigma(I)$]	1512	1064		1101	
no. of parameters	125	112		112	
R1/wR2 [$I \geq 2\sigma(I)$]	0.0364, 0.0949	0.0559, 0.1224		0.0492, 0.1101	
R1/wR2 (all data)	0.0476, 0.1008	0.1018, 0.1350		0.0882, 0.1197	
GOF	0.975	0.928		0.936	
$\Delta\rho$[f] e/Å^3	−0.283, 0.622	−0.549, 1.138		−0.318, 0.879	

[a] Numbers correspond to the Scheme 1. [b] Data were collected after the virgin **1**·2H_2O sample was heated to 360 K at a rate of 2 K/min and cooled down to 298 K at a rate of −10 K/min under a nitrogen atmosphere. [c] Data were collected after **1** was exposed to air at 298 K for 2 h. [d] Data were collected after rehydrated **1-HP** was heated to 360 K at a rate of 2 K/min and cooled down to 298 K at a rate of −10 K/min under nitrogen atmosphere. [e] Data were collected after **1** was kept in the small plastic box with water at 298 K for 1 week. [f] Max and min residual density. [g] This space-group is the same as the symmetry for *Pnma* (No. 62) which is employed for uniform definition of axes with **2S**·2H_2O and **3**·2H_2O.[25,27]

homometallic contacts are longer than 7.9 Å. From the viewpoint of the magnetic dipole interaction, such a short distance describes a ferromagnetic interaction between 2D sheets, which is the situation for **2S**·2H_2O.

Between the 2D sheets the nitrogen atom N(5) of the non-coordinating amine is assumed to be protonated to balance the overall charge. This nitrogen atom is found to have one hydrogen bond (N(5)···O(2), 2.781(11) Å) with

Table 2. Selected Bond Distances, Angles, and Metal Separations for Virgin $1 \cdot 2H_2O$ and Dehydrated **1**

Intranetwork Metal Separations (Å) through One Cyanide Group			
	$1 \cdot 2H_2O$		**1**
Mn(1)···Cr(1)[a]	5.3644(8)	Mn(1)···Cr(1)[a]	5.430(2)
Mn(1)···Cr(1)[#1,b]	5.3814(8)	Mn(1)···Cr(1)[#2,b]	5.276(2)
		Mn(1)···Cr(1)[#3,c]	5.201(3)
Mn(1)···Cr(1) (Ave.)	5.3729(11)	Mn(1)···Cr(1) (Ave.)	5.323(4)

Distances for Hydrogen Bonds (Å)	
	$1 \cdot 2H_2O$
N(5)···O(2)	2.781(11)
O(1)···N(3)[#4]	2.785(3)

[a] Metal separation through C(1)−N(1). [b] Metal separation through C(2)−N(2). [c] Metal separation through C(3)−N(3). [#1] Symmetry codes: $x+1, y, z$. [#2] Symmetry codes: $x, y+1/2, -z+1/2$. [#3] Symmetry codes: $-x+1, -y+1/2, z+1/2$. [#4] Symmetry codes: $x, y, -1+z$.

the oxygen atom of crystal water molecule, but not with the oxygen atom of the coordinated water (N(5)···O(1′), 3.903(9) Å), whereas an intermediate distance of 2.952(4) Å is observed for the corresponding separation in **2S**.$2H_2O$. The oxygen atom O(1) of the coordinating water is found to have two hydrogen bonds with the nitrogen atoms of the cyanide groups from neighboring layer (O(1)···N(3′), 2.785(3) Å). One hydrogen bond is generated by mirror symmetry from the other.

The crystal structure analysis described above revealed a statistical disorder of the diamine ligand on two equivalent crystallographic positions where one is occupied by the *S*-enantiomer and the other by the *R*-enantiomer. Within this model there is a common N(6) atom which has full occupancy and all the other atoms are on half occupancies. N(6) is also the one coordinated to the Mn atom. The structure was solved within the achiral space-group $P2_1/m$. We therefore tested the possibility of finding solutions where the two enantiomers are fully ordered or the compound contains either of the two enantiomers by spontaneous resolution upon crystallization. Search for a doubled unit cell was only successful for $a \times 2b \times c$ but an attempt to do a full structure refinement resulted in locating only the metal ions. Given that the extinctions are similar for both $P2_1$ and $P2_1/m$, we attempted several models using the former but were unsuccessful. When the crystal structure was solved as an *R*- and *S*-enantiomer, the flack parameters were 2.2% and 15.6%, respectively. However, unusual bond lengths, C(6)−C(7) (1.786 Å) and C(5)−N(5) (1.310 Å), were observed. When the crystal structure was refined using both isomers with an adjustable quantity, an acceptable refinement was obtained for $R:S = 53:47$. For all other trial refinements, none of them converged during refinement. The results of these tests indicate the presence of a racemic mixture of the amine and of statistical disorder of the two enantiomers in the crystal structure.

Crystal Structure of 1. The crystal structure of dehydrated **1** was obtained from in situ measurements. The same single crystal used above was heated to 360 K for dehydration and cooled down to 298 K for data collection. All procedures were done in a nitrogen stream. The X-ray structural analyses of the data for dehydrated **1** found the *Pmnb* space-group. The structure consists of a three-dimensional (3D) framework with cyanide connections between the metals (Figure 3). It is formed from similar 2D sheets in the *ab*-plane, discussed above, stacked in a staggered fashion along the *c*-axis. The corrugated sheets slide with respect to their neighbors to introduce the new cyanide bridges, resulting in the new crystal system and symmetry. In the virgin phase, the mirror plane is perpendicular to the *b*-axis and the Cr ion is on an inversion center whereas in the dehydrated phase the mirror planes are perpendicular to the *a*-axis and the Cr ion is on the mirror plane, and *n* glide symmetry is introduced.

After dehydration the coordinating oxygen atom O(1) ($1 \cdot 2H_2O$) is replaced by the nitrogen atom N(3) which belongs to the non-bridging cyanide group in $1 \cdot 2H_2O$. The Mn ion exhibits distorted octahedral geometry comprising nitrogen atoms of five $[Cr(CN)_6]^{3-}$ ions and one nitrogen atom of pnH. Mn(1) has four bridging cyanide nitrogen atoms (N(1), N(2), N(1′) and N(2′)) in equatorial positions, nitrogen atom N(5) from pn, and nitrogen atom N(3) of bridging cyanide from an adjacent layer to complete its octahedral geometry. It should be noted that the coordinating nitrogen atom of the diamine is switched after dehydration, being Mn(1)−N(6) in $1 \cdot 2H_2O$ to Mn(1)−N(5) in **1** (Table 2, Supporting Information, Table S2). This change suggests the existence of structural phase transition which changes the coordination mode of 1,2-diaminopropane, and might be associated with the small peak in the DSC measurement (Supporting Information, Figure S1).

The Mn(1)−N(3) and Mn(1)−N(5) distances of 2.258(6) and 2.437(9) Å, respectively, are longer than the other Mn−N distances (2.191(4)−2.217(4) Å). The observed minimum Mn−N−C and Cr−C−N angles in the cyanide network within the *ab*-plane for **1** of 147.5(5) and 172.8(6)°, respectively, are smaller than the corresponding ones for $1 \cdot 2H_2O$ (162.9(2), 177.2(2)°), describing more distorted crystal structures than $1 \cdot 2H_2O$. Heterometal distances linked by one cyanide group for the dehydrated **1** are shorter (5.201(3) Å) than those of $1 \cdot 2H_2O$ (5.3814(8), 5.3644(8) Å). The disorder of the diamine observed for $1 \cdot 2H_2O$ is also present in the structure of **1**. However, there are now two common atoms, the coordinating nitrogen N(5) and the methyl carbon C(7).

Irreversible Single-Crystal to Single-Crystal and Reversible Single-Crystal to Glass. One of the very unusual observations in the structure determinations described above concerns the reversibility. The as-prepared virgin crystal has a well-ordered structure adopting a monoclinic space-group except for the statistical distribution of the *R*- and *S*-enantiomers. Its transformation to the dehydrated phase is facile and one can determine its structure in a higher orthorhombic symmetry. However, the process is not reversible, and the rehydration of the dehydrated crystal results in a less crystalline phase. More curious is that subsequent dehydration results in the crystalline dehydrated phase which has enough diffraction quality to reveal its crystal structure (Supporting Information, Figure S2, Table S3). This unique situation is associated with the change in the coordination of the

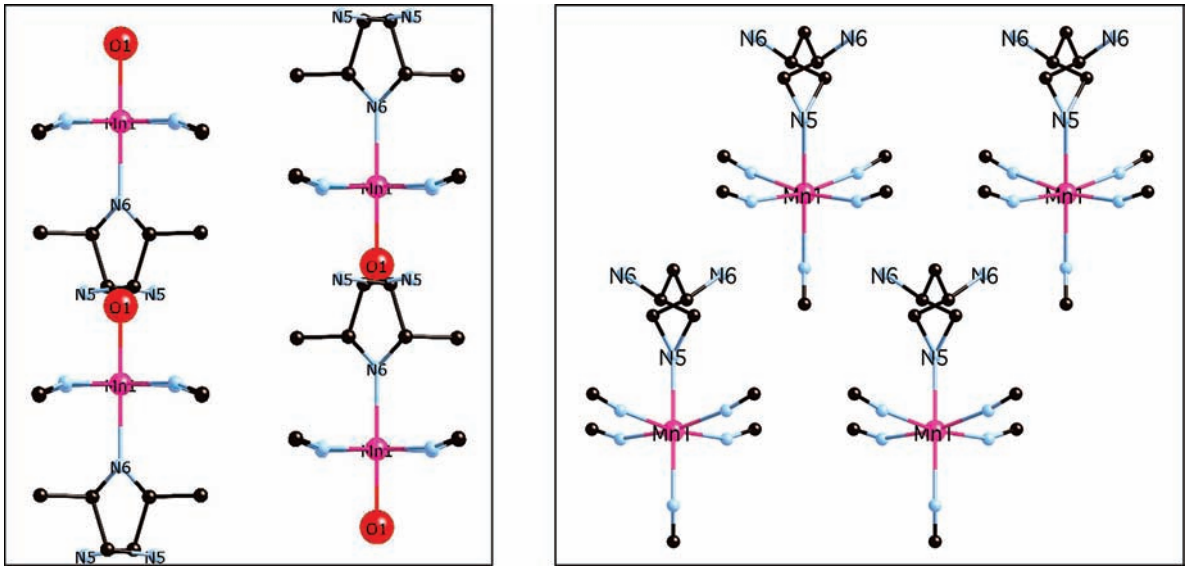

Figure 4. Presentation of the Mn-amine surroundings for $1\cdot 2H_2O$ (left) and **1** (right) showing the only one possible Mn for coordination in $1\cdot 2H_2O$ (left) while there are two equidistant Mn in **1** (right).

amine from one layer to its neighboring ones upon dehydration and rehydration. For this process to take place the positions of the amine with respect to the manganese atoms on adjacent layers must be accessible for coordination. In the virgin crystal, the two disordered nitrogen atoms (from *R*- and *S*-amine) are situated symmetrically next to only one Mn of the adjacent layer as can be seen in Figure 4. Thus upon dehydration there is only one possibility for coordination of N(5) to the Mn. Consequently, the transformation upon the first dehydration results in an ordered arrangement. On the other hand, there are two energetically equivalent Mn atoms in the structure of dehydrated **1** available for the N(6) atom to coordinate. This results in structural disorder and thus causes a poor coherence. It is worthwhile noting that the Curie temperature of the rehydrated **1-HP** is not altered from that of the virgin sample, suggesting that the positions and thus the magnetic exchange pathways between Mn and Cr within each layer are similar (see Magnetic Properties section below).

Powder XRD. To verify the structural change accompanying the dehydration and rehydration, in situ powder XRD patterns for each phase were collected at 298 K. Diffraction data for a virgin sample of $1\cdot 2H_2O$ placed on a glass plate was first collected. The same experiment for dehydrated **1** was performed after the sample had been dehydrated for 10 min at 363 K, then the sample was exposed to air to absorb water molecules for measurement of the diffraction pattern of hydrated **1-HP**. Finally, this phase was dehydrated again by heating to 363 K for 10 min to obtain **1**. The results are shown in Figure 5 and Supporting Information, Figure S3 together with simulated diffraction pattern obtained from the single-crystal data. It is clear that the patterns for both dehydrated phases are the same. However, the pattern for virgin $1\cdot 2H_2O$ and rehydrated **1-HP** show peaks in the same positions, but there is a loss of intensity after rehydration, indicating that the rehydrated phase retains some crystallinity but not enough to performed full Reitveld refinement. However, the close similarity of

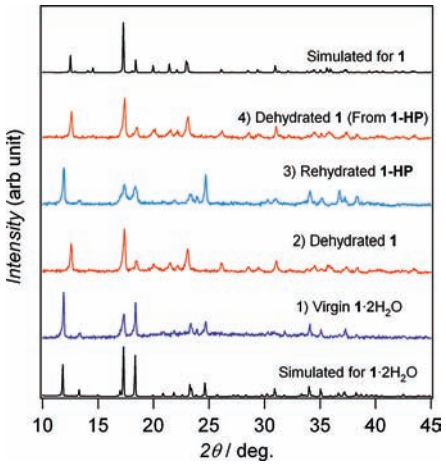

Figure 5. Experimental XRPD patterns for $1\cdot 2H_2O$, **1**, **1-HP**, and **1** (from **1-HP**) using Cu Kα irradiation.

the positions confirms that the heavy atoms are not so perturbed.

Magnetic Properties. Magnetic measurements were performed on several samples from different batches and were found to give similar results (Table 3). The temperature dependences of $\chi_M T$ for virgin $1\cdot 2H_2O$, dehydrated **1**, rehydrated **1-HP**, and dehydrated **1** (from **1-HP**) in a field of 100 Oe are displayed in Figure 6a. The $\chi_M T$ values are 5.09, 4.86, 5.10, and 4.78 cm^3 K mol^{-1} at 300 K, and decrease with lowering temperature down to minimum values of 3.69 (78 K), 3.96 (120 K), 3.72 (78 K), and 3.91 emu K mol^{-1} (114 K), respectively. Upon further cooling, the $\chi_M T$ values increase to maximum values of 921 (31 K), 1830 (52 K), 1212 (30 K), and 1990 (52 K) cm^3 K mol^{-1}, respectively, before decreasing below these temperatures. $\chi_M{}^{-1}$ at high temperatures for each phase follows the Curie−Weiss law ($\chi_M = C/(T-\theta)$) with Weiss constant θ of −65.7, −80.3, −65.4, and −83.0 K and Curie constant C of 6.17, 6.16, 6.20, and 6.11 cm^3 K mol^{-1}, respectively (Figure 6b). These Curie constants are comparable to the theoretical value for the sum of

Table 3. Magnetic Parameters for Virgin $\mathbf{1}\cdot 2H_2O$, Dehydrated **1**, Rehydrated **1-HP** and **1** (from **1-HP**)

	$\mathbf{1}\cdot 2H_2O$	**1**	**1-HP**	**1** (from **1-HP**)
fitting region/K	300−114	360−168	300−114	360−168
R^2 value	0.9999	0.9999	0.9999	0.9997
C^a/cm^3 K mol^{-1}	6.17	6.16	6.20	6.11
θ^b/K	−65.7	−80.3	−65.4	−83.0
$T_{min}{}^c$/K	78	120	78	114
$\chi_M T$ (T_{min})/cm^3 K mol^{-1}	3.69	3.96	3.72	3.91
$\chi_M T$ (300 K)/cm^3 K mol^{-1}	5.09	4.86	5.10	4.78
$T_C{}^d$/K	36	70	36	70
$M_{2\ K}{}^e$/cm^3 G mol^{-1}	396	1550	633	1530
$M_{sat}{}^f/\mu_B$	2.03	2.00	1.99	2.05
$H_C{}^g$/Oe	10	60	10	50
$M_{REM}{}^h/\mu_B$	0.07	0.71	0.10	1.06

[a] Curie constants. [b] Weiss constants. [c] Temperatures at minima of $\chi_M T$. [d] Critical temperatures based on FC measurements. [e] Magnetization at 2 K in FC measurements (H = 5 Oe). [f] Saturation magnetization at 2 K. [g] Coercive field at 2 K. [h] Remnant magnetization at 2 K.

those of Mn(II) and Cr(III): $1/2 \times 5/2 \times 7/2 + 1/2 \times 3/2 \times 5/2 = 6.25$ cm^3 K mol^{-1}. The negative Weiss constants indicate considerable antiferromagnetic interaction between Cr^{III} and Mn^{II} through the cyanide bridge.

In the zero-field-cooled (ZFC) and field-cooled (FC) measurements (Figure 6c) spontaneous magnetization confirming long-range magnetic orderings are observed below 36, 70, 36, and 70 K for virgin $\mathbf{1}\cdot 2H_2O$, dehydrated **1**, hydrated **1-HP**, and dehydrated **1** (from **1-HP**), respectively. The small difference in T_C between $\mathbf{1}\cdot 2H_2O$ and $\mathbf{2S}\cdot 2H_2O$ can be explained by a slight modification of the exchange interaction due to structural differences within the layer. For $\mathbf{2S}\cdot 2H_2O$, the average metal separation between Mn and Cr atom in the 2D sheets (5.3356(19) Å,[25] is shorter than that for $\mathbf{1}\cdot 2H_2O$ (5.3729(11) Å). Therefore, molecular overlap between metal sites involving the cyanide ligand orbitals for $\mathbf{1}\cdot 2H_2O$ is expected to be less than that for $\mathbf{2S}\cdot 2H_2O$; consequently the magnetic ordering is at a lower T_C for $\mathbf{1}\cdot 2H_2O$. For **1** T_C is nearly doubled because of two associated changes; first an increased number of magnetic neighbors through the cyanide group, that is, a change of magnetic dimensionality from 2D to 3D, and second, to shortening of the average distance between Mn and Cr atoms through cyanide group (5.323(4) Å).

A hysteresis loop for each compound was observed at 2 K (Figure 7). The observed saturation magnetization values for virgin $\mathbf{1}\cdot 2H_2O$, dehydrated **1**, hydrated **1-HP**, and dehydrated **1** (from **1-HP**) were 2.03, 2.00, 1.99, and 2.05 μ_B, respectively, and therefore, are in good agreement with the theoretical value for antiparallel alignment of the Cr^{3+} and Mn^{2+} moments ($2 \times 5/2 - 2 \times 3/2 = 2$) assuming $g = 2$ for both metals. The results of spontaneous magnetization and a saturation magnetization of 2 μ_B confirm a collinear ferrimagnetic ground state. The observed remnant magnetizations are 0.07, 0.71, 0.10, and 1.06 μ_B and the coercive fields of the hysteresis loops are 10, 60, 10, and 50 Oe, respectively. These values suggest that $\mathbf{1}\cdot 2H_2O$ is a soft ferrimagnet while it hardens slightly upon dehydration and recovers the initial softness by rehydration.

It is interesting to note that although there is a loss of crystallinity upon rehydration, it does not appear to affect

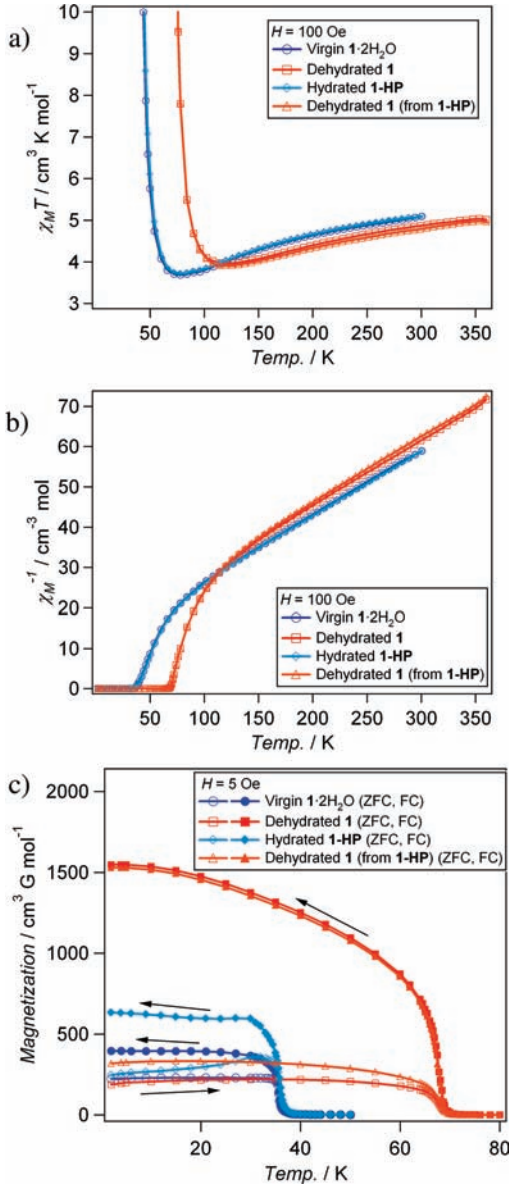

Figure 6. Temperature dependence of (a) $\chi_M T$, (b) $\chi_M{}^{-1}$ and (c) the magnetization in zero field cooled (ZFC) and field cooled (FC) measurement in an applied field of 5 Oe for virgin $\mathbf{1}\cdot 2H_2O$ (circles), dehydrated **1** (squares), rehydrated **1-HP** (diamonds), and **1** (from **1-HP**) (triangles).

the critical temperature of the magnetic ordering or the magnetic hardness from those of the virgin sample. This suggests that there exists the same connectivity and that the magnetic exchange pathways are not altered within the layer as also observed by the powder diffraction and the recovery of the crystallinity upon dehydration.

It is worth comparing the virgin crystal structure and properties of the two compounds containing *rac*-pn coordinating ligand, that is, Mn^{II}−Cr^{III} compound $\mathbf{1}\cdot 2H_2O$ (T_C = 36 K, H_C = 10 Oe) presented in this paper and Mn^{II}−Mn^{III}, $[Mn(rac\text{-pnH})(H_2O)Mn(CN)_6]\cdot 2H_2O$ ($\mathbf{4}\cdot 3H_2O$, T_C = 20.8 K, H_C = 690 Oe), reported by Kaneko et al. in an attempt to derive structure−property relationship.[29] The structures of the two compounds differ in two ways. First, $\mathbf{4}\cdot 3H_2O$, contains two non-coordinating water molecules as opposed to one for $\mathbf{1}\cdot 2H_2O$. Second, the crystal structures are slightly different in the packing of the layers where a [ABAB] sequence is found for

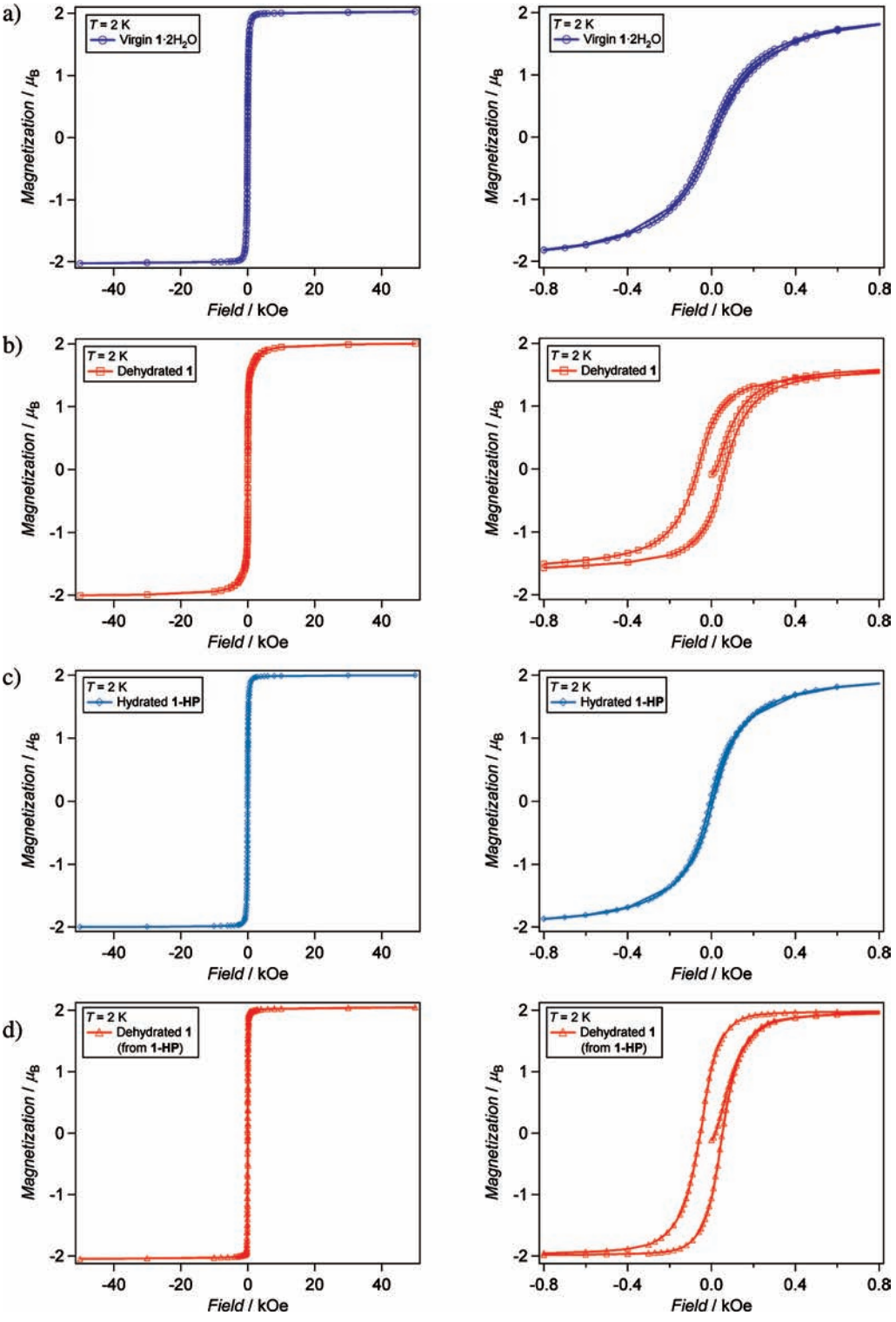

Figure 7. Field dependence of the magnetization at 2 K for (a) virgin $\mathbf{1}\cdot 2H_2O$, (b) dehydrated **1**, (c) rehydrated **1-HP**, and (d) dehydrated **1** (from **1-HP**).

$\mathbf{4}\cdot 3H_2O$, and [AAAA] for $\mathbf{1}\cdot 2H_2O$. Furthermore, $\mathbf{1}\cdot 2H_2O$ appears to have a better mosaicity than $\mathbf{4}\cdot 3H_2O$, and consequently, resulted in a better R1. $\mathbf{1}\cdot 2H_2O$ ($Z = 2$, $V = 833.6(2)$ Å^3) is more voluminous and thus less dense than $\mathbf{4}\cdot 3H_2O$, ($Z = 4$, $V = 1613.1(2)$ Å^3). The difference in the cell volumes is related to the shorter Mn^{III}−C bond distance compared to Cr^{III}−C and is due to the fact that Mn^{III} adopts low-spin $S = 1$ with a d^6 configuration while Cr^{III} has $S = 3/2$ with d^3 configuration. Both compounds behave as ferrimagnets suggesting the prevalence of antiferromagnetic exchange interaction between nearest-neighbors Mn−Cr or Mn−Mn. However, the exchange energy and the Curie temperature of $\mathbf{4}\cdot 3H_2O$ are lower than those of $\mathbf{1}\cdot 2H_2O$. This can be corroborated to the difference in the number of possible interactions and their values between the t_{2g} unpaired electrons of Cr^{III} and Mn^{III} with the Mn^{II} t_{2g} and e_g electrons. This means that electronic interaction is

more important than the distance between the moment carriers. An important factor that Ohba et al. proposed was the introduction of magnetic anisotropy coming from Mn^{III} which is not present for Cr^{III}, resulting in higher coercive field for $\mathbf{4}\cdot 3H_2O$, than for $\mathbf{1}\cdot 2H_2O$.

Conclusion

The irreversible dehydration of a crystal of [Mn(*rac*-pnH)-(H_2O)Cr$(CN)_6]\cdot H_2O$ to a crystal of [Mn(*rac*-pnH)Cr$(CN)_6$] and the consecutive reversible rehydration of a crystal of [Mn(*rac*-pnH)Cr$(CN)_6$] to a glassy [Mn(*rac*-pnH)(H_2O)Cr-$(CN)_6]\cdot H_2O$ were successfully demonstrated through in situ XRD on one single-crystal and by optical and magnetic properties measurements. The transformation upon dehydration is associated with a change of coordination of the diamine from the nitrogen atom on the β-carbon to the one on the α-carbon and from a 2D to 3D network which consequently bring about a change in the Curie temperature from 36 to 70 K. The transformation from either a crystalline or a non-crystalline state to a crystalline one is due to the availability of only one Mn atom for the amine to coordinate whereas that to the less crystalline solid is associated with more Mn atoms in the proximity of the non-coordinated nitrogen of the amine which then results in local disorder and therefore loss of diffraction coherence. Dehydration also brings about an increase of magnetic hardness where the coercive field goes from 10 to 60 Oe. Although [Mn(*rac*-pnH)(H_2O)Cr$(CN)_6]\cdot H_2O$ has similar 2D layered structure and magnetic properties as [Mn(*S*-pnH)(H_2O)Cr$(CN)_6]\cdot H_2O$, they differ on several aspects especially regarding the statistical disorders operating differently under symmetry operations.

Supporting Information Available: Additional information as noted in the text. This material is available free of charge via the Internet at http://pubs.acs.org.